Host Cell Invasion by Trypanosomes Requires Lysosomes and Microtubule/Kinesin–mediated Transport

Ana Rodríguez, Erika Samoff, Marika G. Rioult, Albert Chung, and Norma W. Andrews

Department of Cell Biology, Yale University School of Medicine, New Haven, Connecticut 06510

Abstract. Invasion of mammalian cells by the protozoan parasite *Trypanosoma cruzi* occurs by an actin-independent mechanism distinct from phagocytosis. Clusters of host lysosomes are observed at the site of parasite attachment, and lysosomal markers are detected in the vacuolar membrane at early stages of the entry process. These observations led to the hypothesis that the trypanosomes recruit host lysosomes to their attachment site, and that lysosomal fusion serves as a source of membrane to form the parasitophorous vacuole.

Here we directly demonstrate directional migration of lysosomes to the parasite entry site, using time-lapse video-enhanced microscopy of L_6E_9 myoblasts exposed to *T. cruzi* trypomastigotes. BSA-gold–loaded lysosomes moved towards the cell periphery, in the direction of the parasite attachment site, but only when their original position was less than 11–12 μm from the invasion site. Lysosomes more distant from the invasion area exhibited only the short multi-directional saltatory movements previously described for lysosomes, regardless of their proximity to the cell margins.

Specific depletion of peripheral lysosomes was obtained by microinjection of NRK cells with antibodies against the cytoplasmic domain of lgp 120, a treatment that aggregated lysosomes in the perinuclear area and inhibited *T. cruzi* entry. The microtubule-binding drugs nocodazole, colchicine, vinblastine, and taxol also inhibited invasion, in both NRK and L_6E_9 cells. Furthermore, microinjection of antibodies to the heavy chain of kinesin blocked the acidification-induced, microtubule-dependent redistribution of lysosomes to the host cell periphery, and reduced trypomastigote entry.

Our results therefore demonstrate that during *T. cruzi* invasion of host cells lysosomes are mobilized from the immediately surrounding area, and that availability of lysosomes at the cell periphery and microtubule/kinesin-mediated transport are requirements for parasite entry.

Trypanosoma cruzi, the protozoan parasite that causes Chagas' disease in humans, invades and multiplies in a wide variety of vertebrate cells. The invasion process is unusual, in the sense that it is independent of actin polymerization, and involves the recruitment and fusion of host cell lysosomes at the site of parasite entry (Schenkman et al., 1991; Tardieux et al., 1992; Andrews, 1995). This conclusion is supported by the presence of lysosomal markers in the membrane of partially formed parasite-containing vacuoles (Hall et al., 1992; Tardieux et al., 1992), the colocalization of extracellularly attached parasites with lysosome clusters, and the observation that treatments inducing redistribution of lysosomes from the perinuclear area to the cell periphery enhance invasion. Furthermore, conditions that deplete cells of peripheral lysosomes or impair lysosomal fusion capacity reduce trypanosome entry (Tardieux et al., 1992).

The recruitment of lysosomes, a process apparently triggered by association of *T. cruzi* with host cells before invasion, suggests that the parasite might activate signal transduction pathways involved in lysosome mobilization. Recent reports showed that *T. cruzi* invasion of mammalian cells requires the activation of at least two signaling pathways, one involving phospholipase C–dependent phosphoinositide hydrolysis, with inositol 1,4,5-trisphosphate (IP_3)[1] formation and Ca^{2+} mobilization from intracellular stores (Rodriguez et al., 1995), and another involving the TGF-β I and II receptors (Ming et al., 1995). The IP_3-dependent pathway is triggered by a proteolytically generated trypomastigote factor (PGTF) (Burleigh and Andrews, 1995; Rodriguez et al., 1995) and induces rapid intracellular free Ca^{2+} concentration ($[Ca^{2+}]_i$) transients in mammalian cells (Tardieux et al., 1994; Rodriguez et al., 1995). The relationship between these parasite-induced signals and the

Address all correspondence to N.W. Andrews, Department of Cell Biology, Yale University School of Medicine, 333 Cedar Street, New Haven, CT 06510. Tel.: (203) 785-4314. Fax: (203) 785-7226.

1. *Abbreviations used in this paper*: $[Ca^{2+}]_i$, intracellular free Ca^{2+} concentration; IP_3, inositol 1,4,5-trisphosphate; lgp, lysosomal membrane glycoprotein; NRK, normal rat kidney; PGTF, proteolytically generated trypomastigote factor.

recruitment and fusion of host lysosomes is not fully understood, although we have suggested that Ca^{2+}-triggered cortical actin rearrangements may facilitate lysosome access to the invasion site (Rodriguez et al., 1995).

The movement of lysosomes in mammalian cells is known to be mediated by microtubules, and to be independent of intermediate filaments and microfilament networks (Matteoni and Kreis, 1987). Drugs that affect microtubule stability, such as nocodazole and taxol, inhibit lysosome movement (Herman and Albertini, 1984; Matteoni and Kreis, 1987; Heuser, 1989). Lysosomes and late endosomes are mainly clustered in the perinuclear area, near the slow-growing (minus) end of microtubules (Matteoni and Kreis, 1987; Cole and Lippincott-Schwartz, 1995). Lysosome dispersion towards the cell periphery is observed during mitosis, and can be induced experimentally by microtubule-depolymerizing drugs, or by cytoplasmic acidification. This redistribution is reversible, with rapid reclustering occurring by migration of the lysosomes towards the minus ends of microtubules (Matteoni and Kreis, 1987; Heuser, 1989). Microtubule-associated motor proteins that use the energy of ATP hydrolysis to translocate organelles have been identified, and movements towards the plus and minus ends of microtubules have been attributed, respectively, to kinesin and cytoplasmic dynein (Schroer and Sheetz, 1991).

In this study we use video microscopy to visualize the distribution of lysosomes in living cells during the *T. cruzi* cell entry process. We found that before invasion there is a directional movement of lysosomes located in the vicinity of the entry site towards the parasite attachment site at the cell periphery. Antibody-mediated clustering of lysosomes in the perinuclear area inhibits invasion, suggesting that availability of lysosomes for fusion at the cell periphery is a requirement for parasite entry. In addition, by treating the host cells with drugs that affect microtubule stability, and by microinjecting antibodies that block kinesin function, we show that *T. cruzi* invasion requires an intact microtubule/kinesin-mediated transport apparatus.

Materials and Methods

Materials

Vinblastine, BSA, protein A–Sepharose, protein G–Sepharose, thrombin, and gold chloride were obtained from Sigma Chem. Co. (St. Louis, MO); colchicine, nocodazole, and taxol were from Calbiochem (La Jolla, CA). Lucifer yellow was from Molecular Probes, Inc. (Eugene, OR), and keyhole limpet hemocyanin was from Boehringer Mannheim (Indianapolis, IN).

Mammalian Cells and Parasites

Normal rat kidney (NRK) fibroblasts and L_6E_9 rat myoblasts were grown in DMEM containing 10% FBS, at 37°C with 5% CO_2. Trypomastigotes from the *T. cruzi* Y strain were obtained from the supernatant of infected LLC-MK_2 cells (Andrews et al., 1987). Parasites were washed in Hepes-buffered Ringer's solution (Heuser, 1989) and resuspended in the same solution before exposure to cell monolayers.

Time Lapse Video-enhanced Microscopy

L_6E_9 cells were plated on glass coverslips at 10^4 cells/cm^2 and cultured for 48 h. Lysosomes were labeled by the internalization of BSA adsorbed to 15-nm-gold particles, prepared according to published procedures (Slot and Geuze, 1985). Cells were incubated with BSA-gold (OD 4.0 at 255 nm) for 3 h at 37°C, washed, and chased for 2 h. Coverslips were then mounted in a perfusion chamber (Warner Instruments, New Haven, CT), placed on the heated stage of a Zeiss Axiovert 135 microscope (Carl Zeiss, Inc., Thornwood, NY) and perfused with *T. cruzi* trypomastigotes (5×10^7/ml). Bright-field images were collected using a 100× oil immersion objective, and recorded with a video camera (CCD-C72: Dage/MTI, Michigan City, IN) on an optical memory disc recorder (TQ-3031F, Panasonic, Secaucus, NJ). A computer-controlled shutter system was used to acquire time lapse images at two frames/s (Metamorph software, Universal Imaging, West Chester, PA). Images were transferred to Adobe Photoshop (Adobe Systems, Inc., Mountain View, CA), and composed and printed in a XLS 8600PS high resolution printer (Kodak, Rochester, NY). Lysosome motility tracks were constructed by manually transferring the position of individual lysosomes from the monitor screen onto transparent acetate sheets, during frame by frame playback of the video recording.

Microinjected Antibodies

Anti-lysosomal membrane glycoprotein (lgp) 120 cytoplasmic tail: polyclonal sera were raised by immunizing rabbits with the synthetic peptide R-K-R-S-H-A-G-Y-Q-T-I, corresponding to the conserved hydrophilic COOH-terminal sequence of lgp 120 (Howe et al., 1988; Viitala et al., 1988), coupled to keyhole limpet hemocyanin. IgG isolated from the immune sera with protein A–Sepharose was affinity-purified on the peptide immobilized to ECH Sepharose 4B (Pharmacia Biotech Inc., Pistacaway, NJ). Anti-kinesin: a mouse hybridoma line producing the SUK-4 IgG_1 mAb against kinesin (Ingold et al., 1988) was obtained from the Developmental Studies Hybridoma Bank (Iowa City, Iowa). Culture supernatants were concentrated by ammonium sulfate precipitation and the antibodies affinity purified on protein G–Sepharose.

Microinjection

NRK cells were plated on gridded coverslips (Cellocate, Eppendorf, Madison, WI) at 2×10^4 cell/ml and cultured for 24 h. Coverslips were transferred to DMEM with 1% BSA, 20 mM Hepes, and kept at 37°C on the heated microscope stage during microinjection, which was performed with a microinjector 5242 and micromanipulator 5170 (Eppendorf, Madison, WI). Antibody solutions had a final concentration of 4 mg/ml in microinjection buffer (27 mM K_2HPO_4, 8 mM Na_2HPO_4 and 26 mM KH_2PO_4, pH 7.2). An unrelated IgG_1 mouse mAb was used as a control for SUK-4, and normal rabbit IgG was used as a control for the anti-lgp 120 tail antibodies. Approximately 500 cells were microinjected in each experiment. After injection, the cells were incubated in DMEM 10% FBS at 37°C with 5% CO_2 for 2 h before assays were performed. For acidification-induced redistribution of lysosomes, NRK cells microinjected with SUK-4 mAb or a control IgG_1 mouse mAb were exposed to acetate Ringer's buffer at pH 6.6 (Heuser, 1989) for 15 min before fixation. Lucifer yellow uptake into NRK cells microinjected with anti-lgp 120 tail antibodies was performed by incubation with 10 mg/ml of the tracer in DMEM 10% FBS for 2 h, followed by washes, a chase of 2 h, and fixation.

Cell Invasion Assay

Trypomastigotes were washed in Hepes-buffered Ringer's solution (Heuser, 1989) and resuspended in the same solution at 5×10^7/ml or 2.5×10^7/ml for infection of NRK or L_6E_9 cells, respectively. Coverslips with mammalian cells plated at 2×10^4/cm^2 24 h before were incubated with trypomastigotes for 20 min at 37°C and fixed in 2% paraformaldehyde (PFA) for 20 min. Microtubule inhibitor experiments: host cells were pretreated with the different microtubule inhibitors in DMEM without FBS for 1 h at 37°C. In the case of nocodazole, the cells were preincubated with the drug for 30 min at 4°C, followed by 1 h at 37°C. After infection the cells were fixed and incubated for 30 min with 10 μg/ml IgG from a rabbit immunized with *T. cruzi* trypomastigotes. After washing, rhodamine-conjugated anti–rabbit IgG antibodies (Boehringher Mannheim) were added for 30 min, followed by washing and staining of host cell and parasite DNA with 2.5 μg/ml DAPI (Sigma). With this procedure, only extracellular parasites are stained with rhodamine, while all parasites are stained with DAPI (Tardieux et al., 1992). DAPI-positive parasites with negative or faint rhodamine immunolabeling were counted as intracellular, whereas parasites strongly labeled with anti-*T. cruzi* antibodies were considered extracellular and not counted. More than 200 host cells were analyzed in triplicate for each experiment. Microinjection experiments: NRK cells were infected 2 h after microinjection. After fixation, extracellular parasites were stained with 10 μg/ml IgG from a rabbit immunized with

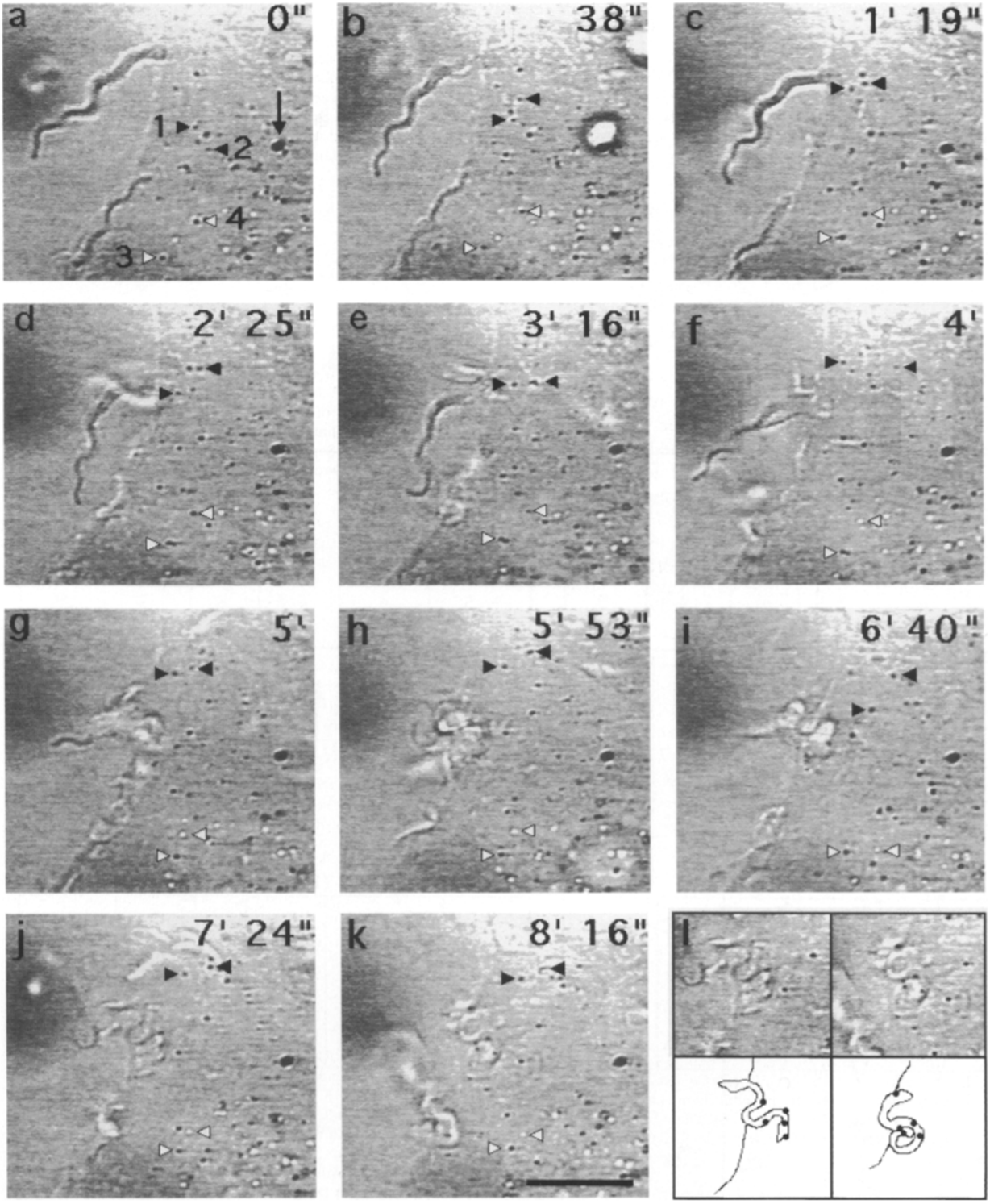

Figure 1. Recruitment of lysosomes during invasion of an L_6E_9 myoblast by *T. cruzi*. (*a–k*) Time lapse images of a trypomastigote entering a cell pre-incubated with BSA-gold for 3 h, followed by a chase of 2 h. Sequential frames are shown approximately every 0.8 min (time indicated in the upper right corner) covering a total period of 8 min. The arrow in *a* points to a fixed reference structure. Black arrowheads (*a*; *1* and *2*) point to two lysosomes that show directional movement towards the parasite attachment site. White arrowheads (*a*; *3* and *4*) point to two lysosomes that did not show directional movement. *k* corresponds to the point at which internalization was completed. (*l*, *upper panels*) Selected areas from *j* and *k* showing the intracellular trypomastigote; (*l*, *lower panels*) schematic representation of the same areas showing BSA-gold–loaded lysosomes associated with the intracellular parasite. Bar, 10 μm.

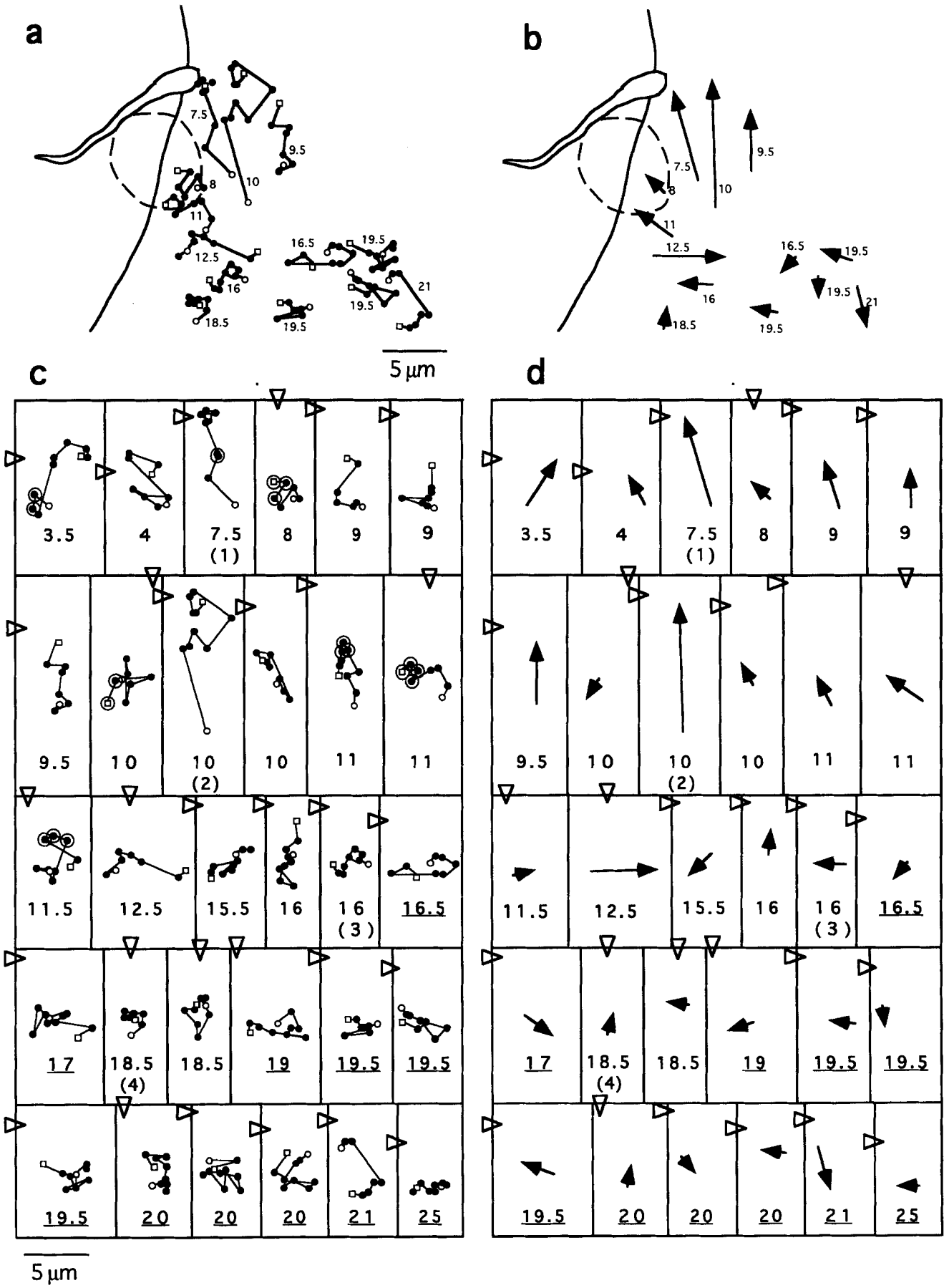
a
b
c
d
5 μm
5 μm
3.5
4
7.5 (1)
8
9
9
9.5
10
10 (2)
10
11
11
11.5
12.5
15.5
16
16 (3)
16.5
17
18.5 (4)
18.5
19
19.5
19.5
19.5
20
20
20
21
25

T. cruzi trypomastigotes followed by incubation with rhodamine-conjugated anti-rabbit IgG antibodies (SUK-4 and control experiments) or with the trypomastigote-specific mAb 2A1 (Andrews et al., 1987) followed by rhodamine-conjugated anti-mouse IgG antibodies (anti-lgp 120 tail and control experiments). After permeabilization with 0.01% saponin, the cells were incubated with fluorescein-conjugated anti-mouse (SUK-4 experiments) or anti-rabbit (anti-lgp 120 tail experiments) IgG (Boeringher Mannheim, Indianapolis, IN) to stain the microinjected antibody. Only parasites associated with microinjected cells were counted; as described above, parasites stained by DAPI and not by extracellularly added anti-*T. cruzi* antibodies were considered intracellular.

Staining for Lysosomes, Endosomes, and Microtubules

Cells were fixed with 2% paraformaldehyde for 15 min, washed in TBS and permeabilized with 0.01% saponin in TBS. To stain microtubules, coverslips were incubated with the TUB 2.1 mAb anti-rat β-tubulin (Sigma), followed by incubation with rhodamine-conjugated anti-mouse IgG antibodies (Boehringher Mannheim) for 30 min. To stain lysosomes, coverslips were incubated with a 1:50 dilution of supernatants from a mouse hybridoma line (LYIC6) producing antibodies to rat lgp 120 (kindly provided by I. Mellman, Department of Cell Biology, Yale University School of Medicine), followed by fluorescein-conjugated anti-mouse IgG antibodies (anti-lgp 120 tail experiments), or affinity-purified anti-lgp 120 tail antibodies followed by fluorescein-conjugated anti-rabbit antibodies (SUK-4 experiments). Microinjected antibodies were stained with either rhodamine-conjugated anti-rabbit IgG or rhodamine-conjugated anti-mouse IgG antibodies. To stain early endosomes, coverslips were incubated with the mAb H68.4 to the cytosolic domain of the human transferrin receptor (White et al., 1992), a gift from I. Trowbridge (Salk Institute, La Jolla, CA), followed by fluorescein-conjugated anti-mouse IgG antibodies. Preparations were visualized in a Zeiss Axiovert 135 fluorescence microscope.

Ca^{2+} Signaling

Soluble extracts of *T. cruzi* trypomastigotes containing the signaling factor PGTF (Rodriguez et al., 1995) were prepared according to published procedures (Burleigh and Andrews, 1995). Spectrofluorometric measurements of $[Ca^{2+}]$; in NRK cells were also performed as described previously (Burleigh and Andrews, 1995).

Results

Host Cell Peripheral Lysosomes Move Directionally Toward the T. cruzi Invasion Site

To study the process of lysosome recruitment by *T. cruzi* trypomastigotes, we selected the L_6E_9 myoblast cell line, since its flat morphology facilitates video-microscopy analysis. Lysosomes were loaded with BSA-gold by fluid-phase endocytosis, and visualized according to the method of De Brabander et al. (1986). When viewed by bright-field microscopy and video-enhanced contrast, lysosomes containing BSA-gold appeared as black spherical structures of relatively uniform size (Figs. 1 and 3). No similar structures were observed in cells not preincubated with BSA-gold (not shown). Trypomastigotes were introduced into the perfusion chamber and kept for 5 min in contact with the cells on the heated microscope stage. The chamber was then perfused with Ringer's solution to wash away unattached parasites, and a field containing trypomastigotes associated with host cell margins was selected for time lapse video recording.

Fig. 1 shows selected frames from a time-lapse recording of one complete sequence of trypomastigote invasion into an L_6E_9 myoblast cell. The invasion process lasted ~8 min;

Table I. Effect of Proximity to the Parasite Entry Site on Lysosome Motility

	Distance traveled (in μm) by individual lysosomes analyzed in Fig. 2									
	48"*	1'36"	2'24"	3'12"	4'	4'48"	5'36"	6'24"	7'12"	8'
3.5‡	1.5	1.3	0.7	[4.2]	0.6	1.6	1.7	0.8	0.2	0.4
4.0	0.6	1.4	1.1	1.1	1.8	[4.5]	0.3	2.4	0.8	0.2
7.5	[3.0]	1.9	0.2	2.6	0.2	0.6	0.5	0.8	0.1	0.6
8.0	0.5	0.8	1.8	0.9	0.1	1.5	0.0	1.1	0.1	0.0
9.0	0.5	0.4	1.3	0.0	0.8	0.1	2.6	0.0	0.1	1.0
9.0	0.5	0.4	0.5	0.5	1.7	2.2	0.5	0.3	0.1	1.9
9.5	0.6	1.3	0.0	1.1	1.8	0.1	0.1	0.0	1.5	2.0
10.0	2.3	1.8	1.6	[3.5]	1.4	1.1	0.1	0.1	1.9	0.0
10.0	[6.2]	0.5	1.2	1.6	[3.2]	[3.2]	0.4	1.5	0.1	1.1
10.0	0.3	1.0	0.8	[3.2]	1.2	1.5	0.5	0.1	0.5	0.3
11.0	1.1	1.5	0.9	1.9	0.8	0.8	0.7	0.1	0.5	0.7
11.0	1.1	1.6	1.2	1.8	0.1	1.0	0.8	0.2	0.0	1.0
11.5	0.1	1.0	1.1	0.8	0.9	2.3	1.2	1.1	[3.2]	0.9
12.5	0.8	1.2	0.7	1.0	1.0	0.0	0.1	[3.2]	0.0	0.9
15.5	0.6	0.6	1.2	0.5	1.2	0.9	0.2	2.0	0.5	0.5
16.0	0.5	0.5	0.6	0.5	1.6	1.3	1.2	0.6	1.1	1.5
16.0	0.6	0.8	0.8	0.8	0.7	0.6	0.7	0.6	0.3	0.7
16.5	0.6	0.5	1.2	1.3	1.5	0.1	1.3	1.9	1.3	1.2
17.0	0.3	0.6	2.1	0.8	1.6	0.5	0.8	0.6	2.9	1.4
18.5	1.2	1.0	0.7	0.7	0.5	0.3	0.0	0.5	0.1	0.5
18.5	0.6	0.3	0.6	0.6	1.8	1.1	1.6	1.0	0.0	0.3
19.0	1.4	1.6	6.0	0.5	1.5	1.1	1.1	1.0	0.7	0.8
19.5	0.6	0.1	0.3	1.5	2.1	0.6	0.2	0.1	0.8	0.7
19.5	0.6	0.2	2.0	0.1	2.1	1.9	1.9	0.1	0.6	0.5
19.5	1.2	0.3	0.3	1.1	1.9	0.7	0.7	1.2	0.6	1.6
20.0	0.6	0.3	0.4	0.3	0.7	1.1	1.1	0.7	1.6	1.2
20.0	2.1	1.7	0.3	0.5	1.7	1.6	1.6	1.9	1.4	1.4
20.0	0.7	0.3	1.6	0.6	1.6	0.7	1.3	0.9	1.1	1.1
21.0	0.6	0.5	[4.1]	0.6	0.1	0.8	0.4	0.0	0.6	0.6
25.0	0.3	0.2	0.4	0.5	0.4	1.0	1.0	0.1	0.3	0.3

*Time intervals in which the distance of each lysosome from its position in the previous time frame was measured, starting with the frame shown in Fig. 1 *a*. The total period analyzed was 8 min.

‡Original distance of each individual lysosome to the parasite attachment site, as indicated in Fig. 2. Boxed numbers indicate distances equal to or longer than 3 μm.

Figure 2. Directional movement of BSA-gold–loaded lysosomes towards the *T. cruzi* invasion site. (*a*) Diagram showing the frame-to-frame trajectory of thirteen selected lysosomes, during the 8-min time interval corresponding to the invasion sequence shown in Fig. 1, *a–k*. Small open circles and squares represent, respectively, the initial and final position of each lysosome. The distance in μm from each lysosome to the parasite attachment site in the initial frame (Fig. 1 *a*) is indicated next to each track. The dotted circle indicates the area into which the parasite moved when cell invasion was initiated (Fig. 1, *f–h*). *b*, same as *a*, except that the frame-to-frame tracks were replaced by arrows indicating the direction of movement of each lysosome; the base and tip of the arrows correspond, respectively, to the initial and final position of each lysosome. (*c* and *d*) Diagrams showing the linear tracks and corresponding directions of movement of all thirty individual lysosomes analyzed. Large open circles represent the frames in which lysosomes colocalized with the parasite. The distance in μm from each lysosome to the parasite attachment site in the initial frame (Fig. 1 *a*) is indicated below each track; underlined numbers indicate lysosomes originally located at more than 10 μm from the cell margin. Numbers in parentheses indicate the lysosomes shown by arrowheads in Fig. 1 *a*. Open triangles represent the initial position of the parasite in relation to each lysosome (Fig. 1 *a*).

frames are shown approximately every 0.8 min (Fig. 1, *a–k*). During this period, the movements of all lysosomes that were continuously in focus were tracked by recording their position in relation to a reference structure (Fig. 1 *a*, *arrow*). Black arrowheads in Fig. 1 point to two lysosomes (#1, #2) that showed significant directional movement, covering a distance of more than 7 μm towards the parasite attachment site (Fig. 1, *a–e*). White arrowheads point to two lysosomes (#3, #4) that did not show directional movement during the same period.

Analysis of the position of lysosomes #1 and #2 in relation to the reference structure (Fig. 1, *arrow*) shows that the most significant directional movement occurred between frames *a* and *d*, during a period of ~2.5 min that followed the stable attachment of the trypomastigote to the host cell margin, and before cell invasion was initiated. Mean velocities of 0.055 μm/s and 0.135 μm/s were calculated for lysosomes #1 and #2, respectively, during this period. These values are within the range reported previously for the velocity of intracellular vesicles traveling on microtubules (Herman and Albertini, 1984; Matteoni and Kreis, 1987). After lysosomes #1 and #2 reached the cell periphery, their movement was significantly reduced (Fig. 1, *f*, *black arrowheads*), and their motility pattern in the remaining frames (Fig. 1, *g–k*, *black arrowheads*) resembled the short-range saltatory movement showed by lysosomes #3 and #4 throughout the whole invasion sequence (Fig. 1, *a–k*, *white arrowheads*). Lysosome #1 associated transiently with the invading trypomastigote (Fig. 1, *c–e*), although this particular lysosome did not fuse with the nascent parasitophorous vacuole and continued to move forward (Fig. 1, *f–k*). However, some gold-loaded lysosomes did appear to fuse with the parasitophorous vacuole, as indicated by the accumulation of BSA-gold particles observed around the parasite at later stages of the entry process (Fig. 1 *l*).

For a more quantitative assessment of lysosome movement in relation to the invading parasite, the movements of all lysosomes continuously in focus throughout the complete invasion sequence shown in Fig. 1 were individually tracked. The trajectory of some of these lysosomes in relation to the attached parasite is shown in Fig. 2 *a*. The initial and final positions and the direction of movement of the same lysosomes are represented by the arrows in Fig. 2 *b*. Fig. 2, *c* and *d* shows trajectories and direction of movement for all lysosomes analyzed in this video sequence, a total of thirty. Lysosomes originally located closer to the invasion site tended to move towards the host cell periphery, in direction of the parasite attachment site (Fig. 2, *b* and *d*). The arrows indicating the initial and final position

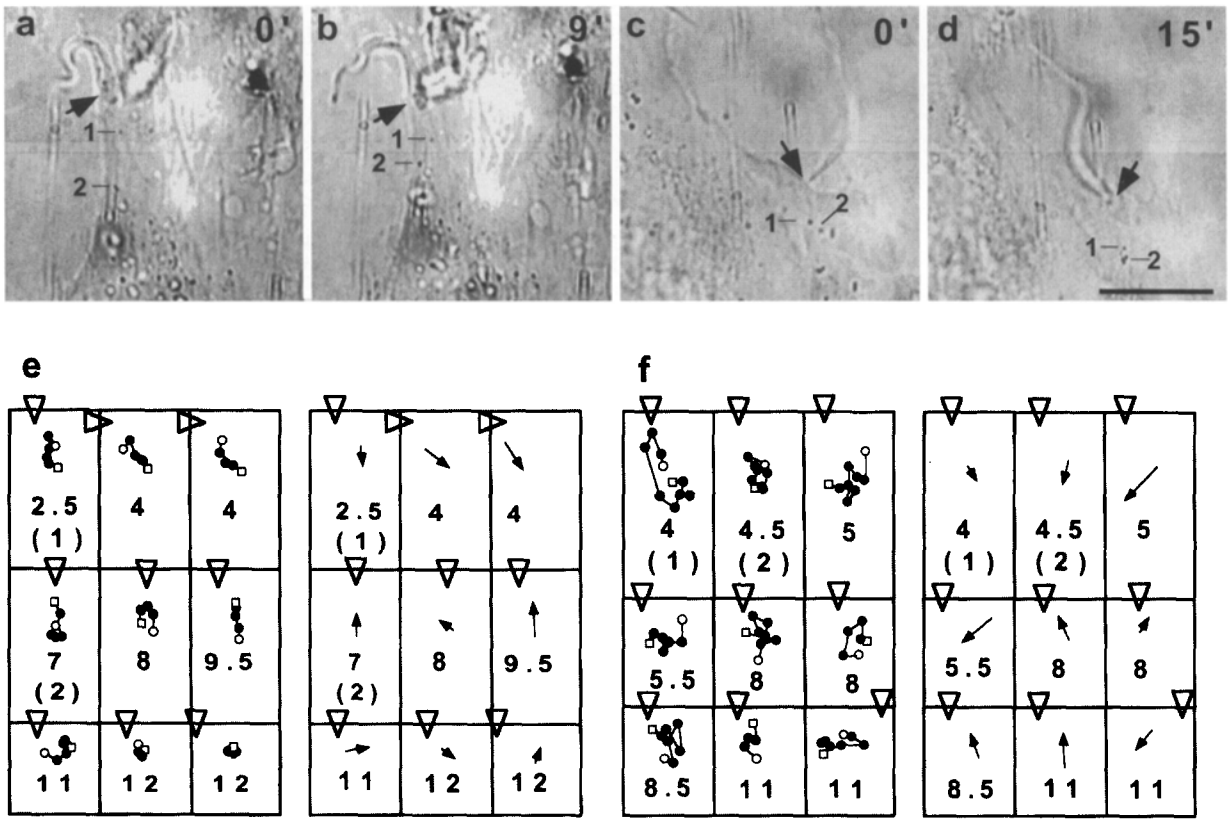

Figure 3. Parasite attachment not followed by invasion does not induce lysosome recruitment. Initial (*a* and *c*) and final (*b* and *d*) frames of two independent time lapse image recordings of trypomastigote attachment events that did not result in invasion. L_6E_9 myoblasts were pre-incubated with BSA-gold for 3 h, followed by a chase of 2 h. The *a–b* sequence covered a period of 9 min, and the *c–d* sequence a period of 15 min. Black lines indicate the initial (*a* and *c*) and final (*b* and *d*) positions of two lysosomes (*1* and *2*) in each sequence. The arrows point to the trypomastigote attachment site. (*e* and *f*) Trajectory and direction of movement of nine individual lysosomes during the *a–b* (*e*) and *c–d* (*f*) recorded sequences, as described in the legend of Fig. 2. All lysosomes in both video recordings were originally <10 μm from the cell margin. Bar, 10 μm.

of each lysosome (Fig. 2 *d*) show that when initial distances to the invasion site were shorter than 12 μm (distance in μm is indicated by the numbers below each track/arrow), eleven out of thirteen lysosomes underwent directional movement.

From the eleven video frames analyzed (Fig. 1, *a–k*), the initial five (Fig. 1, *a–e*) correspond to events occurring before the trypomastigote entered the host cell. We can therefore conclude that long stretches of directional lysosome movement occurred before invasion, while the parasite was still attached to the host cell margin (Table I, time frames 48″–3′12″). Measurements of the distance traveled during regular time intervals (every 0.8 min) revealed nine instances of dislocations longer than 3 μm, for lysosomes originally at less than 12 μm from the invasion site. In contrast, when lysosomes originally at more than 12 μm from the invasion site were analyzed, only two were found to move more than 3 μm between selected frames (Table I, *boxed numbers*).

The lysosomes located at >12 μm from the invasion site showed mostly the short saltatory movements previously described for these organelles (Herman and Albertini, 1984; Matteoni and Kreis, 1987). This motility pattern appeared to be independent of the distance of the lysosomes to the host cell margin, as can be verified in Fig. 2 (where underlined numbers designate lysosomes originally at more than 10 μm from the cell margin) and Fig. 3 (where all lysosomes analyzed were at less than 10 μm from the cell margin).

These findings strongly suggest that the recruitment of lysosomes occurring before and during *T. cruzi* invasion involves only lysosomes initially located at the host cell periphery, in the vicinity of the entry site. Furthermore, transient attachment of trypomastigotes to host cells that do not result in internalization do not appear to affect the motility of lysosomes in the surrounding area. This can be observed in Fig. 3, which shows the analysis of lysosome motility in two independent video recordings of parasite attachments that did not result in invasion (*a–b* and *c–d* correspond to the first and last frame of each recording). Lysosomes in the vicinity of the parasite attachment site showed only random saltatory movements with no preferential direction (Fig. 3, *e* and *f*). In addition, distances traveled by individual lysosomes in these cells every 0.8 min were all shorter than 3 μm, similar to what was observed for distant lysosomes in the "productive" invasion sequence (Table II, compare with Table I).

Table II. Lysosome Motility in Cells with Attached but Noninvading Parasites

Distance traveled (in μm) by individual lysosomes analyzed in Fig. 3 *e*.										
	48″*	1′36″	2′24″	3′12″	4′	4′48″	5′36″	6′24″	7′12′	8′
2.5‡	0.5	0.3	0.0	0.1	0.2	0.0	0.1	0.0	0.5	0.1
4.0	0.1	0.5	0.1	0.1	0.2	0.0	0.3	0.5	0.0	0.0
4.0	0.6	0.0	0.3	0.0	0.1	0.1	0.0	0.1	0.1	0.7
7.0	0.7	0.2	0.4	0.0	0.1	0.0	0.6	0.0	0.2	0.7
8.0	1.0	0.1	0.5	0.0	0.1	0.2	0.0	0.0	0.2	0.3
9.5	0.6	0.1	0.1	0.2	0.3	0.0	0.2	0.1	0.0	0.2
11.0	0.8	0.5	0.0	0.5	0.1	0.5	0.3	0.3	0.0	0.1
12.0	0.2	0.0	0.1	0.0	0.0	0.3	0.0	0.3	0.0	0.0
12.0	0.0	0.2	0.0	0.2	0.0	0.0	0.2	0.2	0.1	0.3

Distance traveled (in μm) by each individual lysosome analyzed in Fig. 3 *f*.										
	48″*	1′36″	2′24″	3′12″	4′	4′48″	5′36″	6′24″	7′12″	8′
4.0‡	0.6	1.0	2.6	0.1	1.1	0.7	0.2	0.4	0.1	0.3
4.5	1.1	0.2	0.3	0.0	0.5	0.2	0.0	0.1	0.2	0.4
5.0	1.5	0.0	0.7	0.1	1.1	0.0	0.1	0.3	0.1	0.0
5.5	1.2	0.9	0.0	0.2	0.1	0.2	0.0	0.0	0.0	0.8
8.0	0.1	0.7	0.0	0.7	0.3	0.1	0.1	0.2	0.3	1.3
8.0	0.9	0.1	0.0	0.0	0.0	1.2	1.1	0.3	0.0	0.0
8.5	0.5	0.1	0.1	0.0	0.6	0.1	0.5	0.2	0.0	0.1
11.0	0.0	0.1	0.1	0.6	0.3	0.0	0.1	1.0	0.1	0.1
11.0	0.5	0.0	1.3	0.1	0.0	0.2	0.1	0.0	0.1	0.0

*Time intervals in which the distance of each lysosome from its position in the previous time frame was measured, starting with the frames shown in Fig. 3 *a* (*top table*) or 3 *c* (*bottom table*). The total period analyzed was 8 min.
‡Original distance of each individual lysosome to the parasite attachment site, as indicated in Fig. 3, *e* and *f*. No dislocation was longer than 3 μm.

Antibodies to the Cytoplasmic Tail of lgp 120 Induce Aggregation of Lysosomes and Inhibit T. cruzi Invasion

The time lapse video microscopy observations described above showed that peripheral lysosomes are gradually mobilized to the vicinity of the trypomastigote invasion site. To obtain direct evidence that this recruitment of lysosomes is required for *T. cruzi* invasion, we sought an irreversible method of removing lysosomes from the host cell periphery without affecting the distribution of other organelles. For this we took advantage of the high concentration of the glycoprotein lgp 120 in lysosomes. Lgp 120, together with the related lgp 110, accounts for ~50% of the total protein content of lysosomal membranes. It has a heavily glycosylated lumenal domain, a single transmembrane anchor, and a short, highly conserved eleven amino acid cytoplasmic tail (Kornfeld and Mellman, 1989). We prepared affinity-purified polyclonal antibodies against a synthetic peptide corresponding to the cytoplasmic tail of lgp 120, and microinjected these antibodies into NRK fibroblasts. As a control, normal rabbit IgG was injected into a separate group of cells.

Immunofluorescence with anti–rabbit antibodies was used to visualize the microinjected IgG (Fig. 4, *a* and *b*). To stain lysosomes of both injected and noninjected cells, labeling with a mAb specific for the lumenal domain of rat lgp 120 was performed on the same preparations (Fig. 4, *c* and *d*). Cells injected with normal IgG showed a diffuse distribution of the microinjected antibody throughout the cytoplasm (Fig. 4 *a*). The general distribution of lysosomes in these cells appeared normal, indistinguishable from noninjected cells in the same field (Fig. 4 *c*). In contrast, in cells injected with anti-lgp 120 tail IgG, the antibodies were visualized associated with large structures (Fig. 4 *b*), which also stained with the mAb against the lumenal domain of lgp 120 (Fig. 4 *d*). Thus, the introduction of anti-lgp 120 tail antibodies induced a dramatic reorganization in the distribution of lysosomes, with the formation of large clusters in the perinuclear area. A similar aggregation of lysosomes by microinjected anti-lgp 120 tail antibodies was observed in L_6E_9 rat myoblasts and in HeLa cells (not shown).

Since trace amounts of lgp 120 have been detected in early endosomes (Rabinowitz et al., 1992), we investigated

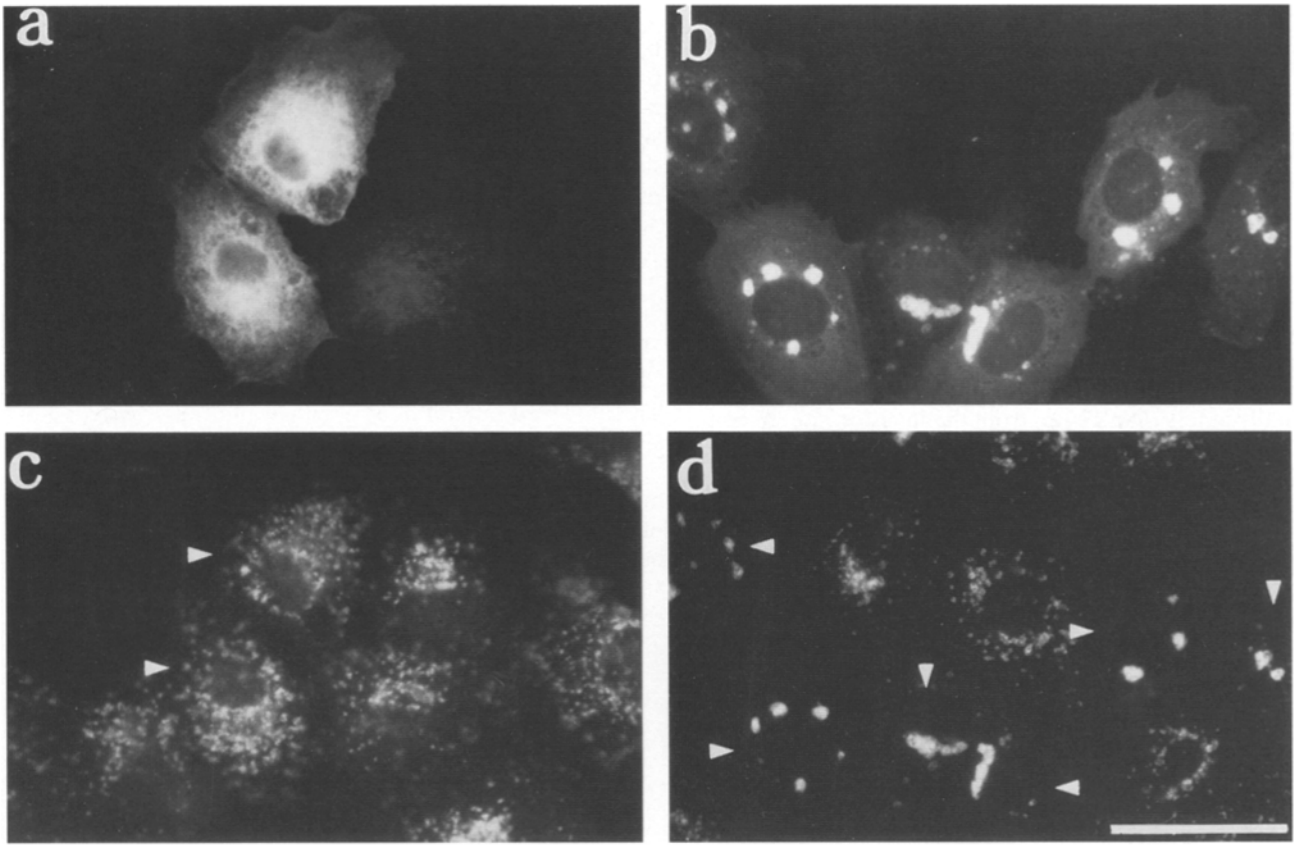

Figure 4. Microinjection of anti-lgp 120 tail antibodies into NRK cells induces clustering of lysosomes. (*a*) Cells microinjected with normal rabbit IgG, stained with anti–rabbit IgG secondary antibody. (*c*) same field as *a*, stained with an mAb to the lumenal domain of rat lgp 120; arrowheads point to microinjected cells, showing a normal lysosome distribution. (*b*) Cells microinjected with affinity-purified antibodies to the cytoplasmic domain of lgp 120, stained with anti–rabbit IgG secondary antibody; (*d*) same field as *b*, stained with an mAb to the lumenal domain of rat lgp 120; arrowheads point to microinjected cells, showing clustered lysosomes. Bar, 10 μm.

if the distribution of transferrin receptor-containing compartments was affected by microinjection of anti-lgp 120 tail antibodies. As shown in Fig. 5, no changes were detected in the distribution of transferrin receptor-containing compartments after microinjection of anti-lgp 120 tail antibodies, with no colocalization of the aggregated structures (Fig. 5 *a*) and the compartments containing transferrin receptor (Fig. 5 *b*). These observations indicate that the anti-lgp 120 tail antibodies only induce clustering of compartments containing lgp in high density, namely late endosomes and lysosomes. Further confirming this interpretation, we found that lucifer yellow taken up by fluid phase endocytosis colocalized with the antibody-clustered lysosomes after a 2-h chase period (Fig. 5, *c* and *d*). Since the fluid phase tracer was added to the medium after the antibody-induced aggregation of lysosomes, this experiment also demonstrates that traffic from early endosomes into lysosomes is not affected by the binding of antibodies to the cytosolic domain of lgp 120.

Immunofluorescence images showed that there was a significant reduction in the number of free lysosomes at the periphery of NRK cells microinjected with the anti-lgp tail antibodies (Fig. 4, *b* and *d*, Fig. 6, *b* and *d*). Therefore, we used this system to evaluate the requirement for peripheral lysosomes in host cell invasion by *T. cruzi*. When compared with the infection rates of control cells, anti-lgp 120 tail-injected cells contained a reduced number of intracellular parasites. Lower infectivity was observed in three independent experiments, with an average decrease of 44.4% (Table III). The few parasites found inside cells microinjected with anti-lgp 120 tail were surrounded by membranes reactive with the injected antibodies and with a mAb against lgp 120 lumenal domain (Fig. 6, *a–c*). Therefore, entry of these parasites was probably mediated by fusion of lysosomes that escaped agglutination by the anti-lgp tail antibodies. Small lysosome clusters and a few structures that may correspond to free lysosomes were indeed detectable in the periphery of microinjected cells (Fig. 6 *d*).

T. cruzi Invasion Requires Intact Microtubules

The association between *T. cruzi* invasion and lysosome mobilization suggested a requirement for microtubule-mediated transport. Inhibition of microtubule function and stability, and therefore vesicle transport, can be achieved in mammalian cells by treatment with nocodazole, vinblastine, colchicine (Luduena and Roach, 1991), or taxol (Hamm-Alvarez et al., 1993). NRK and L_6E_9 cells were pretreated with the irreversible drugs colchicine, vinblastine, and taxol, or with the reversible drug nocodazole, and invasion assays were performed. Nocodazole was kept in

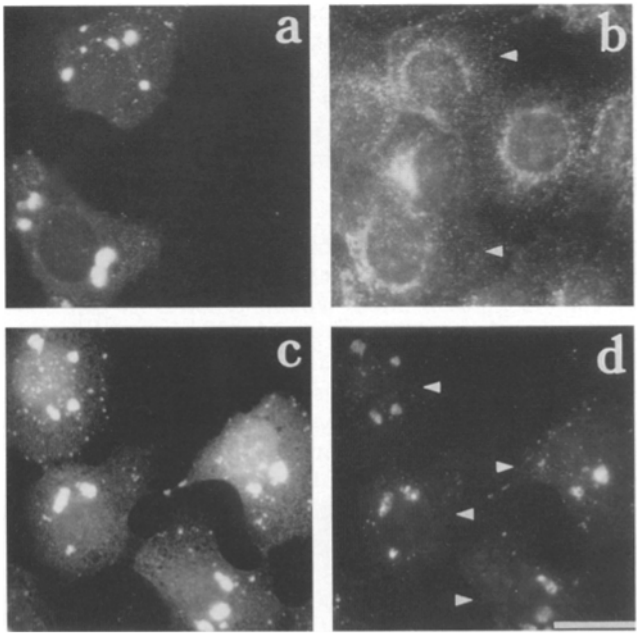

Figure 5. Anti-lgp 120 tail antibody induces clustering of lysosomes but not of early endosomes. (*a* and *b*) The distribution of transferrin receptor-containing early endosomes is not altered in NRK cells with clustered lysosomes: (*a*) cells microinjected with anti-lgp 120 tail antibodies, stained with anti–rabbit secondary antibody; (*b*) same field as *a*, stained with an mAb to the transferrin receptor; arrowheads point to microinjected cells. (*c* and *d*) Endocytosed lucifer yellow is delivered to clustered lysosomes after a 2-h chase: (*c*) cells microinjected with anti-lgp 120 tail antibodies, stained with anti–rabbit secondary antibody; (*d*) same field as *c*, showing lucifer yellow fluorescence in the clustered lysosomes; arrowheads point to microinjected cells. Bar, 5 μm.

the medium during the invasion assay, since it is known not to affect trypanosome microtubules (Tardieux et al., 1992; Robinson et al., 1995).

In both NRK and L_6E_9 cells, the number of trypomastigotes invading drug-treated cells was significantly reduced in relation to untreated cells (Fig. 7). The inhibition induced by colchicine was dose-dependent, and correlated well with the degree of microtubule depolymerization observed in the cells by immunofluorescence with anti-β tubulin (not shown).

Table III. Anti-lgp 120 Tail Antibodies Inhibit Host Cell Invasion by T. cruzi

Control (parasites/100 cells)	Anti-lgp tail (parasites/100 cells)	Inhibition of invasion
		%
18.8	6	68.0
18.7	11.2	40.2
16.0	11.9	25.3
		mean 44.4 ± 21.6 SD

T. cruzi invasion was quantitated in ~200 microinjected cells, identified by labeling microinjected antibodies with fluorescein-conjugated anti–rabbit IgG. Total parasites were localized by DAPI staining and intracellular parasites by absence of staining, before cell permeabilization, with a mAb to a trypomastigote membrane protein followed by rhodamine-conjugated anti–mouse IgG. Only parasites associated with microinjected cells were counted. SD, standard deviation.

To verify if treatment with microtubule-active drugs under our experimental conditions affected the availability of signaling receptors at the plasma membrane, NRK cells treated with 10 μM colchicine for 1 h were tested in a Ca^{2+} signaling assay. The agonists used were thrombin and *T. cruzi* soluble extracts containing the Ca^{2+}-signaling factor PGTF, previously implicated in host cell invasion (Burleigh and Andrews, 1995; Rodriguez et al., 1995). We found that colchicine treatment did not block the generation of $[Ca^{2+}]_i$ transients in NRK cells after exposure to either one of the factors (not shown).

Anti-kinesin Antibodies Inhibit T. cruzi Invasion

The observed migration of lysosomes to the *T. cruzi* invasion site at the cell periphery (Figs. 1 and 2) suggested the involvement of a microtubule-based, plus-end directed motor such as kinesin. Inhibition of kinesin-driven motility of organelles has been achieved with mAbs to the kinesin heavy chain, either in vitro (Ingold et al., 1988; Brady et al., 1990) or after introduction of the antibodies into intact cells (Hollenbeck and Swanson, 1990). To investigate if inhibitory antibodies to kinesin interfered with lysosome anterograde movement and *T. cruzi* invasion, NRK cells were microinjected with SUK-4 mAb (Ingold et al., 1988) or an unrelated IgG_1 mAb.

To demonstrate that the microinjected SUK-4 antibodies were effective in inhibiting kinesin-dependent lysosomal movements under our conditions, we used cytosolic acidification as an assay for microtubule-dependent anterograde transport (Heuser, 1989). Kinesin heavy chain has been shown to be involved in the acidification-induced redistribution of lysosomes to the periphery of mammalian cells (Feiguin et al., 1994; Nakata et al., 1995). In cells injected with control antibodies, immunofluorescent staining of lysosomes revealed the expected redistribution of lysosomes to the cell periphery after acidification (Fig. 8, *e* and *f*). In contrast, in cells microinjected with the SUK-4 anti-kinesin mAb the lysosomes remained clustered in the perinuclear area after acetate treatment (Fig. 8, *g–j*). Microinjection of either control (Fig. 8, *a* and *b*) or SUK-4 (Fig. 8, *c* and *d*) mAbs had no effect on the normal perinuclear organization of lysosomes in cells kept at neutral pH.

Susceptibility to infection by *T. cruzi* was measured after microinjection of control and SUK-4 anti-kinesin antibodies in NRK cells. Five different experiments were performed, and inhibition ranging from 35.2 to 69.4% was observed, when controls were compared with SUK-4–injected cells (Table IV). Also consistent with a role for the ATP-driven motor kinesin in *T. cruzi* invasion, we observed a 52% reduction in parasite entry into NRK cells pretreated with sodium azide (10 mM, 30 min at 37°C). This treatment has been described to deplete in 90% the cellular pool of ATP, and to completely arrest the saltatory motion of intracellular vesicles (De Brabander et al., 1988).

Discussion

We have characterized the recruitment of lysosomes that occurs during the invasion of mammalian cells by the protozoan parasite *T. cruzi.* Previous studies (Hall et al., 1992;

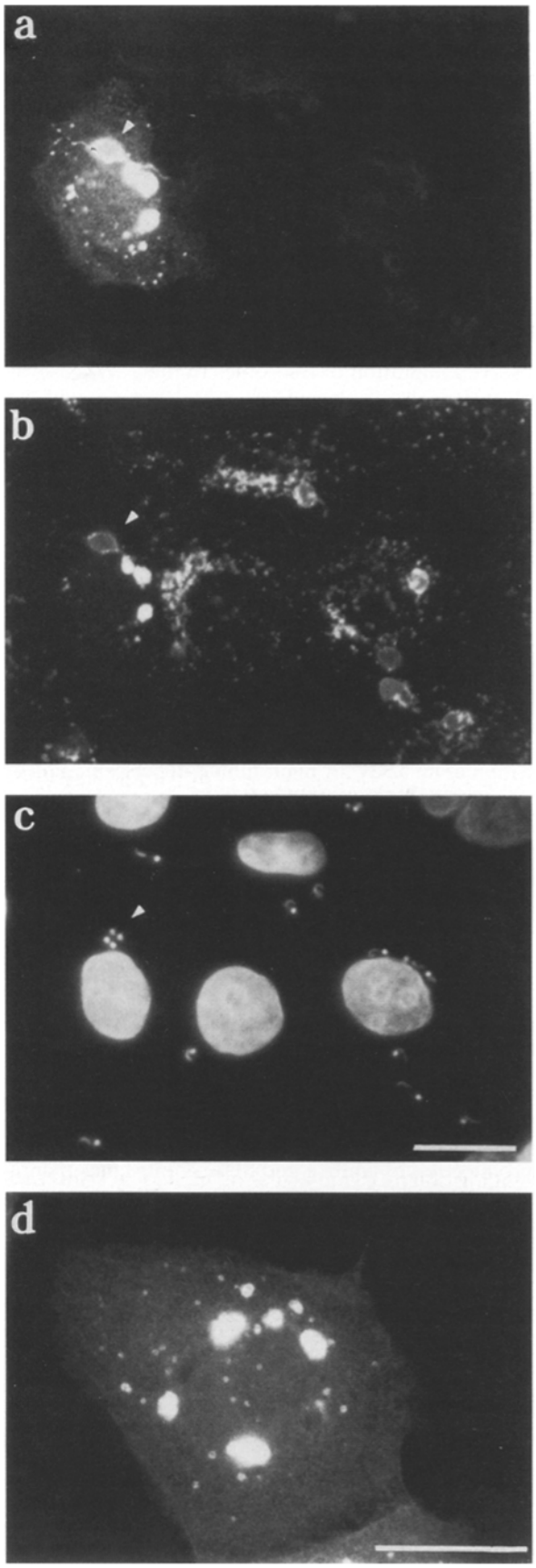

Tardieux et al., 1992) had detected clusters of lysosomes at the sites of parasite attachment and lysosomal markers in partially formed parasitophorous vacuoles, suggesting migration and fusion of lysosomes at the invasion site. However, actual mobilization of lysosomes to the plasma membrane could not be detected in those studies because they involved fixed preparations.

We now followed by video-enhanced time lapse microscopy the distribution of lysosomes in living L_6E_9 myoblasts, from the time of stable parasite attachment to that of complete internalization. We found that BSA-gold containing lysosomes gradually accumulated around the invading parasite, and that this accumulation resulted from a directional migration of lysosomes originally present at the host cell periphery. Analysis of the invasion sequence in Fig. 1 showed that eleven out of thirteen lysosomes present in an area at less than 12 μm from the invasion site moved towards the cell periphery, in direction of the parasite attachment area. Of these eleven lysosomes, eight traveled more than 3 μm from their initial to final position. Two of the lysosomes in this group moved more than 7 μm in the direction of the parasite, and one of them remained associated with the trypomastigote attachment site for several min (Fig. 1, *a–e*, lysosome #1). In contrast, seventeen randomly selected lysosomes in areas at more than 12 μm of the invasion site exhibited only short movements in each direction (Fig. 2).

Earlier scanning electron microscopy studies showed that *T. cruzi* trypomastigotes invade mammalian cells predominantly at the cell periphery (Schenkman et al., 1988). The video microscopy studies described here confirm this view, since all complete invasion sequences observed started with the attachment of trypomastigotes to lamellar extensions at the cell margins. However, several instances of attachment of trypomastigotes to cell margins that did not result in the invasion were also observed. These "unproductive" parasite attachments did not induce directional movement of lysosomes. Therefore, our observations suggest that localized signals may be generated by parasites once they become stably attached, resulting in mobilization of lysosomes from the surrounding area.

Although a direct involvement of Ca^{2+} signaling in lysosome recruitment by *T. cruzi* has not been demonstrated, previous studies showed that trypomastigotes induce rapid, IP_3-mediated $[Ca^{2+}]_i$ transients in a variety of mammalian cells, and that inhibition of these transients blocks

Figure 6. Residual invasiveness of cells microinjected with anti-lgp 120 antibodies involves lysosome fusion. (*a–c*) NRK cells infected with *T. cruzi* trypomastigotes. (*a*) Cell microinjected with affinity-purified antibodies to the cytoplasmic domain of lgp 120, stained with anti–rabbit IgG secondary antibody; (*b*) same field as *a*, stained with a mAb to the lumenal domain of rat lgp 120; (*c*) same field as *a*, stained for DNA with DAPI (parasites stain as two dots, corresponding to the nucleus and kinetoplast). The arrowhead in *a–c* points to two trypomastigotes that invaded a microinjected cell, and that are inside a vacuole reactive with anti-lgp antibodies. Additional parasite-containing vacuoles positive for lgp staining can be seen in the noninjected cells shown in *b*. (*d*) Close-up of an NRK cell microinjected with antibodies to the cytoplasmic domain of lgp 120, showing the incomplete clustering of the lysosomes. Bars, 5 μm.

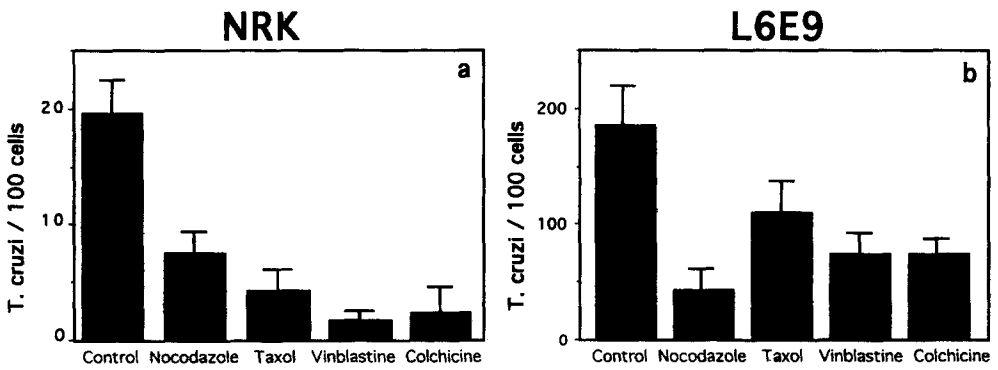

Figure 7. Inhibitors of host cell microtubule dynamics reduce *T. cruzi* invasion. The number of intracellular parasites in NRK (*a*) or L_6E_9 cells (*b*) pretreated with microtubule inhibitors was determined after a 20-min infection period. Drug concentrations in *a* and *b* were 10 μM nocodazole, 4 μM taxol, 1 μM vinblastine, and 10 μM colchicine. The data represent the average of triplicate determinations ±SD.

parasite entry (Tardieux et al., 1994; Rodriguez et al., 1995). Interestingly, a localized area of elevated $[Ca^{2+}]_i$ was detected around recently internalized *T. cruzi* trypomastigotes in L_6E_9 myoblasts (Moreno et al., 1994). Since a soluble Ca^{2+}-signaling factor extracted from trypomastigotes (PGTF) is capable of inducing a rapid and reversible disassembly of the cortical actin cytoskeleton of NRK cells (Rodriguez et al., 1995), it is conceivable that a localized, Ca^{2+} triggered microfilament rearrangement induced by live parasites is a required step for migration and fusion of lysosomes during formation of the *T. cruzi*-containing vacuole.

The observation that only lysosomes in the vicinity of the invasion site are recruited may be related to the spatial dynamics of locally induced second messengers. Although the cytosolic range of action for Ca^{2+} is very short (~0.08 μm), IP_3 has a longer diffusion length, estimated in the cytoplasm of *Xenopus* oocytes to be ~17 μm (Kasai and Petersen, 1994). This value is compatible with the 11–12 μm range of action for lysosome mobilization detected in our study, further reinforcing a possible relationship between the *T. cruzi*-induced, IP_3-mediated Ca^{2+} signal (Rodriguez et al., 1995) and lysosome recruitment. cAMP, in contrast, has been reported to have a diffusion length of 30–220 μm (Kasai and Petersen, 1994), significantly longer than the range of directional lysosome motility observed during *T. cruzi* invasion.

Several lines of evidence suggest that lysosomes approaching the trypomastigote invasion site gradually fuse with the plasma membrane, contributing to formation of the parasitophorous vacuole. In addition to the gradual accumulation of BSA-gold around invading trypanosomes observed in this study, lgp 120 and 3-h chased horseradish peroxidase were detected in partially formed vacuoles, when portions of the parasites were still extracellular (Hall et al., 1992; Tardieux et al., 1992). In this context, the behavior of lysosome #1 in the time lapse invasion sequence shown in Fig. 1 was intriguing. It moved with an average velocity of 0.05 μm/s towards the parasite attachment site, where it remained for ~2 min before detaching and reassuming a saltatory pattern of movement at a location above the invasion site. This transient association followed by detachment is very similar to what was reported for the interaction of BSA-gold–containing late endosomes with phagosomes in macrophages (Desjardins et al., 1994). One possibility is that these observations are related to the loading of lysosomes with BSA-gold, since the presence of certain indigestible substances within lysosomes and phagolysosomes can interfere with their fusion capacity (Montgomery et al., 1991; Oh and Swanson, 1996). On the other hand, differential rates of transfer of distinct soluble fluorescent tracers from lysosomes to phagolysosomes have been described (Wang and Goren, 1987), suggesting that transient fusion-fission events, referred to as "kiss and run" (Desjardins, 1995), might occur. Since fluorescent tracers can only be used to follow the movement of intracellular organelles for a limited period of time, due to the damage of vesicular membranes that occurs upon illumination (De Brabander et al., 1986; Swanson et al., 1992), we did not attempt to repeat our invasion studies using fluorescent markers.

To interfere specifically with the availability of lysosomes for fusion at the cell periphery and test its effect on trypanosome invasion, we microinjected NRK cells with antibodies against the conserved, eleven amino acid cytoplasmic tail of the major lysosome membrane glycoprotein lgp 120. These antibodies induced a dramatic clustering of lysosomes in the perinuclear area, significantly reducing the number of isolated lgp-positive structures detectable at the cell periphery. This is, to our knowledge, the first demonstration that the cytoplasmic domain of lgp 120 is exposed on the surface of lysosomes, and accessible to antibody binding in living cells. The aggregation of lysosomes induced by the antibodies was most probably due to cross-linking of lgp 120 molecules on individual lysosomes, as would be predicted by the estimated high density of lgp in lysosomal membranes (Granger et al., 1990).

Three independent invasion assays performed on NRK cells 2 h after microinjection of anti-lgp 120-tail antibodies revealed a reduction ranging from 25 to 68% in the number of internalized trypomastigotes. We believe this variation can be explained by the variable degrees of lysosome aggregation achieved (Figs. 4 *b* and 6 *d*), since it is not possible to reproduce precisely the final concentration of antibodies introduced by microinjection. The few intracellular parasites found inside anti-lgp tail-injected cells were surrounded by a vacuolar membrane reactive with the injected antibodies. This observation indicates that successful invasion events still involved lysosome fusion, and that binding of antibodies to the cytoplasmic domain of lgp 120 did not block fusion. Furthermore, we found that lucifer yellow taken up by fluid phase endocytosis was delivered

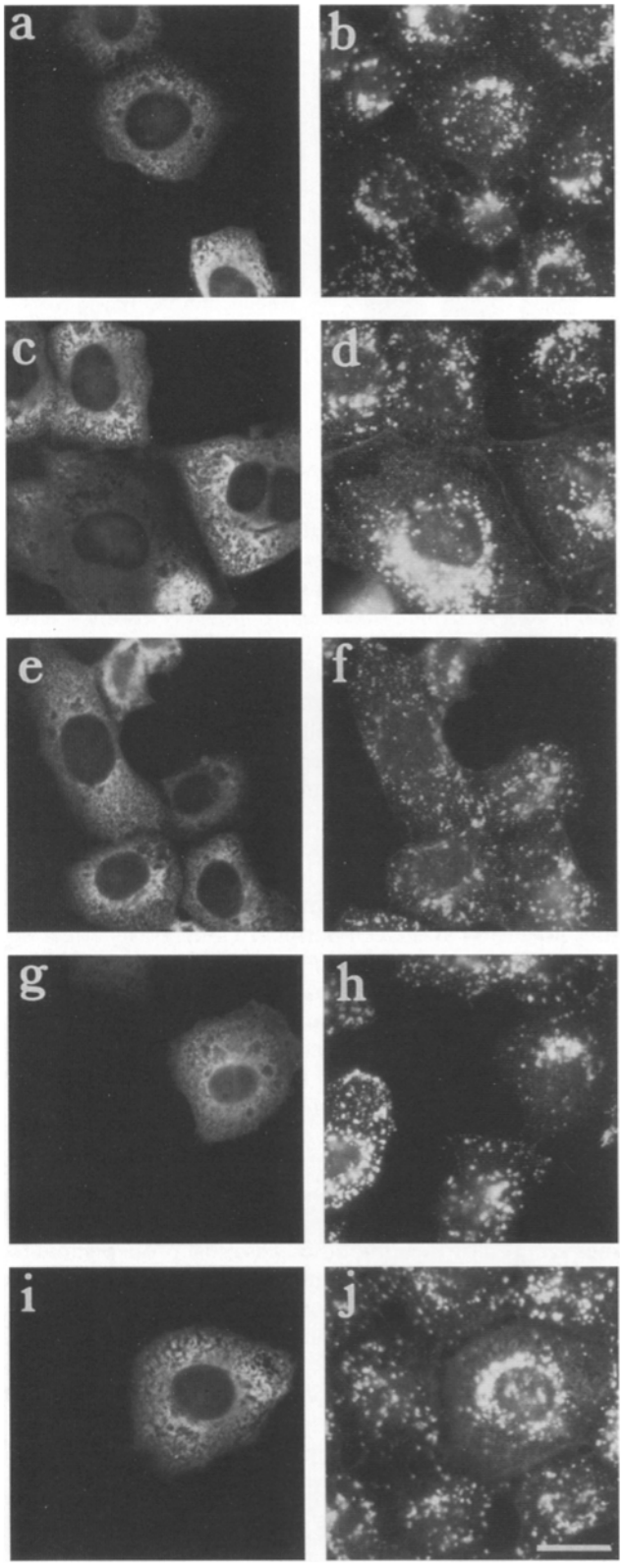

Figure 8. Microinjection of anti-kinesin antibodies blocks the acidification-induced redistribution of lysosomes in NRK cells. Cells were microinjected with control mouse IgG_1 (*a*, *b*, *e*, and *f*) or SUK-4 anti-kinesin (*c*, *d*, *g*, *h*, *i*, and *j*) and exposed to pH 7.0 (*a–d*) or pH 6.6 (*e–j*) buffers before fixation and staining of lysosomes. The acidification-induced movement of lysosomes away from the cell center, observed in cells injected with the control antibody (*e* and *f*) was blocked by SUK-4 (*g* and *h*). Another example is shown in (*i* and *j*) where a single cell injected with SUK-4 shows a perinuclear distribution of lysosomes while the noninjected cells surrounding it show the acidification-induced redistribution (*j*). Bar, 5 μm.

Table IV. Anti-Kinesin Antibodies Inhibit Host Cell Invasion by T. cruzi

Control (parasites/100 cells)	Anti-kinesin (parasites/100 cells)	Inhibition of invasion
		%
32	12	62.5
29.3	18.9	35.5
9.1	5.9	35.2
9.2	4.3	53.3
19.3	5.9	69.4
		mean 51 ± 13.9 SD

T cruzi invasion was quantitated in ~200 microinjected cells, identified by labeling microinjected antibodies with fluorescein-conjugated anti–mouse IgG. Total parasites were localized by DAPI staining and intracellular parasites by absence of staining, before cell permeabilization, with rabbit anti-*T. cruzi* specific antiserum followed by rhodamine-conjugated anti–rabbit IgG. Only parasites associated with microinjected cells were counted. SD, standard deviation.

to the antibody-clustered lysosomes after a 2-h chase. We therefore favor the hypothesis that the reduced susceptibility to *T. cruzi* infection of cells injected with anti-lgp 120 tail antibodies is due to decreased availability of lysosomes at the cell periphery, and not to a block in lysosome fusion. Another possibility is that the movement of aggregated lysosomes, and therefore their recruitment to the invasion site, was impaired. Experiments using cytosolic acidification showed that the larger the particles contained in lysosomes, the more reduced was their capacity to move towards the plus-end of microtubules (Perou and Kaplan, 1993).

The requirement for lysosome mobilization during *T. cruzi* invasion strongly suggested an involvement of host cell microtubules. Earlier experiments designed to address this question were inconclusive, since treatment of NRK cells with nocodazole failed to inhibit infection (Tardieux et al., 1992). In the present study we found that effective depolymerization of NRK cell microtubules with nocodazole requires a pre-incubation period at 4°C, as described for polarized epithelial cells (Hunziker et al., 1990). Under these conditions, significant inhibition of *T. cruzi* entry was observed in both NRK fibroblasts and L_6E_9 myoblasts. Host cells were also exposed to two other microtubule-active drugs with different mechanisms of action, colchicine, and vinblastine (Luduena and Roach, 1991), and both significantly reduced entry of the parasite in the two cell lines tested. Inhibition was also observed with the stabilizing agent taxol, shown to interfere with certain microtubule-mediated vesicular transport steps in mammalian cells (Herman and Albertini, 1984; Hamm-Alvarez et al., 1993). Our results therefore demonstrate a requirement for host cell microtubule dynamics in the *T. cruzi* invasion process.

Microtubule-binding drugs such as taxol have been reported to interfere with the recycling of signaling receptors to the plasma membrane (Hamm-Alvarez et al.,

1994). Since there is evidence that *T. cruzi* invasion involves receptor-mediated, parasite-induced Ca^{2+} signaling (Tardieux et al., 1994; Rodriguez et al., 1995), the reduction in invasion by microtubule inhibitors could have been related to depletion of cell surface receptors. We verified, however, that after treatment with 10 μM colchicine (a dose that inhibits *T. cruzi* invasion of NRK cells by 90%) there was no block of the $[Ca^{2+}]_i$ transients triggered by the trypomastigote soluble factor PGTF (Rodriguez et al., 1995). In addition, receptor-mediated Ca^{2+} signaling triggered in NRK cells by the well-characterized agonist thrombin was also not inhibited by colchicine, under the same conditions.

The outward migration of lysosomes observed during trypomastigote invasion suggested involvement of the plus end–directed microtubule motor kinesin. This was confirmed by the reduced parasite entry in cells microinjected with the inhibitory anti-kinesin mAb SUK-4 (Ingold et al., 1988; Hollenbeck and Swanson, 1990). Kinesin activity is regulated by Ca^{2+}-calmodulin in vitro (Matthies et al., 1993), which raises the possibility that PGTF-induced Ca^{2+} signaling may play a role in localized lysosome motility by direct modulation of motor activity. Since the lysosome motility patterns we observed were quite complex, involving both anterograde and retrograde movements, it is conceivable that the minus end–directed motor cytoplasmic dynein is also involved. Binding of cytoplasmic dynein to lysosomes was shown to depend on the presence of Ca^{2+} in the extracellular medium (Lin and Collins, 1993).

Recruitment and fusion of lysosomes with the plasma membrane has been described as part of the exocytic pathway of specialized cells, such as neutrophils and cytotoxic lymphocytes (Pryzwansky et al., 1979; Griffiths and Argon, 1995). In these cell types, fusion of lysosome-related granules with the plasma membrane is triggered by Ca^{2+} (Poenie et al., 1987; Jaconi et al., 1990). Cytotoxic T cell granules were shown to move along microtubules in a kinesin-dependent fashion (Burkhardt et al., 1993), and in neutrophils, a localized disassembly of actin filaments was detected at the site of fusion of azurophil granules with the plasma membrane (Boyles and Bainton, 1981). This report, and our previous finding that a *T. cruzi* soluble factor induces Ca^{2+}-dependent disassembly of the cortical actin cytoskeleton of NRK fibroblasts (Rodriguez et al., 1995), suggest an intriguing parallel between regulated exocytosis and the recruitment of lysosomes during trypanosome invasion of mammalian cells.

We thank D. Johnston for affinity purification of anti-lgp 120 tail antibodies, B. Kowalsky and D. Johnston for help with the initial microinjection experiments, P. Male and H. Tan for photography, and A. Ma for production of parasites and excellent technical assistance. We are also grateful to B. Burleigh, T. Kreis and M. Rabinovitch for helpful discussions and comments on the manuscript.

This work was supported by the National Institutes of Health RO1AI34867 grant to N.W. Andrews. A. Rodriguez was the recipient of a fellowship from CYCIT (Spain) and E. Samoff was supported by the National Institutes of Health Molecular Parasitology grant 5T32 AIO7404.

Received for publication 29 January 1996 and in revised form 16 April 1996.

References

Andrews, N.W. 1995. Microbial subversion of phagocytosis: lysosome recruitment during host cell invasion by *Trypanosoma cruzi*. *Trends Cell Biol.* 5: 133–137.

Andrews, N.W., K.S. Hong, E.S. Robbins, and V. Nussenzweig. 1987. Stage-specific surface antigens expressed during the morphogenesis of vertebrate forms of *Trypanosoma cruzi*. *Exp. Parasitol.* 64:474–484.

Boyles, J., and D.F. Bainton. 1981. Changes in plasma-membrane-associated filaments during endocytosis and exocytosis in polymorphonuclear leukocytes. *Cell.* 24:905–914.

Brady, S.T., K.K. Pfister, and G.S. Bloom. 1990. A monoclonal antibody against kinesin inhibits both anterograde and retrograde fast axonal transport in squid axoplasm. *Proc. Natl. Acad. Sci. USA.* 87:1061–1065.

Burkhardt, J.K., J.M. McIlvain, M.P. Sheetz, and Y. Argon. 1993. Lytic granules from cytotoxic T cells exhibit kinesin-dependent motility on microtubules in vitro. *J. Cell Sci.* 104:151–162.

Burleigh, B., and N.W. Andrews. 1995. A 120 kDa alkaline peptidase from *Trypanosoma cruzi* is involved in the generation of a novel Ca^{2+}-signaling factor for mammalian cells. *J. Biol. Chem.* 270:5172–5180.

Cole, N.B., and J. Lippincott-Schwartz. 1995. Organization of organelles and membrane traffic by microtubules. *Curr. Opin. Cell Biol.* 7:55–64.

De Brabander, M., R. Nuydens, G. Geuens, M. Moeremans, and J. De May. 1986. The use of submicroscopic gold particles combined with video contrast enhancement as a simple molecular probe for the living cell. *Cell Motil. Cytoskeleton.* 6:105–113.

De Brabander, M., R. Nuydens, H. Geerts, and C.R. Hopkins. 1988. Dynamic behavior of the transferrin receptor followed in living epidermoid carcinoma (A431) cells with nanovid microscopy. *Cell Motil. Cytoskeleton.* 9:30–47.

Desjardins, M. 1995. Biogenesis of phagolysosomes: the 'kiss and run' hypothesis. *Trends Cell Biol.* 5:183–186.

Desjardins, M., L.A. Huber, R.G. Parton, and G. Griffiths. 1994. Biogenesis of phagolysosomes proceeds though a sequential series of interactions with the endocytic apparatus. *J. Cell Biol.* 124:677–688.

Feiguin, F., A. Ferreira, K.S. Kosik, and A. Caceres. 1994. Kinesin-mediated organelle translocation revealed by cellular manipulations. *J. Cell Biol.* 127: 1021–1039.

Granger, B., S.A. Green, C.A. Gabel, C.L. Howe, I. Mellman, and A. Helenius. 1990. Characterization and cloning of lgp 110, a lysosomal membrane glycoprotein from mouse and rat cells. *J. Biol. Chem.* 265:12036–12043.

Griffiths, G.M., and Y. Argon. 1995. Structure and biogenesis of lytic granules. *Curr. Top. Microbiol. Immunol.* 198:39–58.

Hall, B.F., P. Webster, A.K. Ma, K.A. Joiner, and N.W. Andrews. 1992. Desialylation of lysosomal membrane glycoproteins by *Trypanosoma cruzi*: a role for the surface neuraminidase in facilitating parasite entry into the host cell cytoplasm. *J. Exp. Med.* 176:313–325.

Hamm-Alvarez, S.F., P.Y. Preston, and M.P. Sheetz. 1993. Regulation of vesicle transport in CV-1 cells and extracts. *J. Cell Sci.* 106:955–966.

Hamm-Alvarez, S.F., B.E. Alayof, H.M. Himmel, P.Y. Kim, A.L. Crews, H.C. Strauss, and M.P. Sheetz. 1994. Coordinate depression of bradykinin receptor recycling and microtubule-dependent transport by taxol. *Proc. Natl. Acad. Sci. USA.* 91:7812–7816.

Herman, B., and D.F. Albertini. 1984. A time-lapse video intensification analysis of cytoplasmic organelle movements during endosome translocation. *J. Cell Biol.* 98:565–576.

Heuser, J.E. 1989. Changes in lysosome shape and distribution correlated with changes in cytoplasmic pH. *J. Cell Biol.* 108:855–864.

Hollenbeck, P.J., and J.A. Swanson. 1990. Radial extension of macrophage tubular lysosomes supported by kinesin. *Nature (Lond.).* 346:864–866.

Howe, C.L., B.L. Granger, M. Hull, S.A. Green, C.A. Gabel, A. Helenius, and I. Mellman. 1988. Derived protein sequence, oligosaccharides, and membrane insertion of the 120 kDa lysosomal membrane glycoprotein (lgp 120): identification of a highly conserved family of lysosomal membrane glycoproteins. *Proc. Natl. Acad. Sci. USA.* 85:7577–7581.

Hunziker, W., P. Male, and I. Mellman. 1990. Differential microtubule requirements for transcytosis in MDCK cells. *EMBO (Eur. Mol. Biol. Organ.) J.* 9: 3515–3525.

Ingold, A.L., S.A. Cohn, and J.M. Scholey. 1988. Inhibition of kinesin-driven microtubule motility by monoclonal antibodies to kinesin heavy chains. *J. Cell Biol.* 107:2657–2667.

Jaconi, M.E.E., D.P. Lew, J.L. Carpentier, K.E. Magnusson, M. Sjogren, and O. Stendahl. 1990. Cytosolic free calcium elevation mediates the phagosome-lysosome fusion during phagocytosis in human neutrophils. *J. Cell Biol.* 110: 1555–1564.

Kasai, H., and O.H. Petersen. 1994. Spatial dynamics of second messengers: IP_3 and cAMP as long-range and associative messengers. *Trends Neurosci.* 17: 95–101.

Kornfeld, S., and I. Mellman. 1989. The biogenesis of lysosomes. *Annu. Rev. Cell Biol.* 5:483–525.

Lin, S.X.H., and C.A. Collins. 1993. Regulation of the intracellular distribution of cytoplasmic dynein by serum factors and calcium. *J. Cell Sci.* 105:579–588.

Luduena, R.F., and M.C. Roach. 1991. Tubulin sulfhydryl groups as probes and targets for antimitotic and antimicrotubule agents. *Pharmac. Ther.* 49:133–152.

Matteoni, R., and T.E. Kreis. 1987. Translocation and clustering of endosomes and lysosomes depends on microtubules. *J. Cell Biol.* 105:1253–1265.

Matthies, H.J.G., R.J. Miller, and H.C. Palfrey. 1993. Calmodulin binding to and cAMP-dependent phosphorylation of kinesin light chains modulate kinesin ATPase activity. *J. Biol. Chem.* 268:11176–11187.

Ming, M., M.E. Ewen, and M.A. Pereira. 1995. Trypanosome invasion of mammalian cells requires activation of the TGFβ signaling pathway. *Cell.* 82:1–20.

Montgomery, R.R., P. Webster, and I. Mellman. 1991. Accumulation of indigestible substances reduces fusion competence of macrophage lysosomes. *J. Immunol.* 147:3087–3095.

Moreno, S.N., J. Silva, A.E. Vercesi, and R. Docampo. 1994. Cytosolic free calcium elevation in *Trypanosoma cruzi* is required for invasion. *J. Exp. Med.* 180:1535–1540.

Nakata, T., and N. Hirokawa. 1995. Point mutation of adenosine triphosphate-binding motif generated rigor kinesin that selectively blocks anterograde lysosome membrane transport. *J. Cell Biol.* 131:1039–1053.

Oh, Y-K., and J.A. Swanson. 1996. Different fates of phagocytosed particles after delivery into macrophage lysosomes. *J. Cell Biol.* 132:585–593.

Perou, C.M., and J. Kaplan. 1993. Chediak-Higashi syndrome is not due to a defect in microtubule-based lysosomal mobility. *J. Cell Sci.* 106:99–107.

Poenie, M., R.Y. Tsien, and A.M. Schmitt-Verhulst. 1987. Sequential activation and lethal hit by $[Ca^{2+}]_i$ in individual cytolytic T cells and targets. *EMBO (Eur. Mol. Biol. Organ.) J.* 6:2223–2232.

Pryzwansky, K.B., E.K. MacRae, J.K. Spitznagel, and M.H. Cooney. 1979. Early degranulation of human neutrophils: immunocytochemical studies of surface and intracellular phagocytic events. *Cell.* 18:1025–1033.

Rabinowitz, S., H. Horstmann, S. Gordon, and G. Griffiths. 1992. Immunocytochemical characterization of the endocytic and phagolysosomal compartments in peritoneal macrophages. *J. Cell Biol.* 116:95–112.

Robinson, D.R., T. Sherwin, A. Ploubidou, E.H. Byard, and K. Gull. 1995. Microtubule polarity and dynamics in the control of organelle positioning, segregation, and cytokinesis in the trypanosome cell cycle. *J. Cell Biol.* 128: 1163–1172.

Rodríguez, A., M.G. Rioult, A. Ora, and N.W. Andrews. 1995. A trypanosome-soluble factor induces IP_3 formation, intracellular Ca^{2+} mobilization and microfilament rearrangement in host cells. *J. Cell Biol.* 129:1263–1273.

Schenkman, S., N.W. Andrews, V. Nussenzweig, and E.S. Robbins. 1988. *Trypanosoma cruzi* invade a mammalian epithelial cell in a polarized manner. *Cell.* 55:157–165.

Schenkman, S., E.S. Robbins, and V. Nussenzweig. 1991. Attachment of *Trypanosoma cruzi* to mammalian cells requires parasite energy, and invasion can be independent of the target cell cytoskeleton. *Infect. Immun.* 59:645–654.

Schroer, T.A., and M.P. Sheetz. 1991. Functions of microtubule-based motors. *Annu. Rev. Physiol.* 53:629–652.

Slot, J.W., and H.J. Geuze. 1985. A new method of preparing gold probes for multiple-labeling cytochemistry. *Eur. J. Cell Biol.* 38:87–93.

Swanson, J.A., A. Locke, P. Ansel, and P. Hollenbeck. 1992. Radial movement of lysosomes in permeabilized macrophages. *J. Cell Sci.* 103:202–209.

Tardieux, I., P. Webster, J. Ravensloot, W. Boron, J.A. Lunn, J.E. Heuser, and N.W. Andrews. 1992. Lysosome recruitment and fusion are early events required for trypanosome invasion of mammalian cells. *Cell.* 71:1117–1130.

Tardieux, I., M. Nathanson, and N.W. Andrews. 1994. Role in host cell invasion of *Trypanosoma cruzi*-induced cytosolic-free Ca^{2+} transients. *J. Exp. Med.* 179:1017–1022.

Viitala, J., S.R. Carlsson, P.D. Siebert, and M. Fukuda. 1988. Molecular cloning of cDNAs encoding lamp A, a human lysosomal membrane glycoprotein with apparent Mr ~ 120,000. *Proc. Natl. Acad. Sci. USA.* 85:3743–3747.

Wang, Y.L., and M.B. Goren. 1987. Differential and sequential delivery of fluorescent lysosomal probes into phagosomes in mouse peritoneal macrophages. *J. Cell Biol.* 104:1749–1754.

White, S., K. Miller, C. Hopkins, and I.S. Trowbridge. 1992. Monoclonal antibodies against defined epitopes of the human transferrin receptor cytoplasmic tail. *Biochim. Biophys. Acta.* 1136:28–34.